John von Neumann Institute for Computing

Density Functional Modeling of Magnesia Supported Pd Clusters: On the Road to an Understanding of Nanoscale Catalysis

B. Huber, P. Koskinen, H. Häkkinen, M. Moseler

published in

NIC Symposium 2008,
G. Münster, D. Wolf, M. Kremer (Editors),
John von Neumann Institute for Computing, Jülich,
NIC Series, Vol. **39**, ISBN 978-3-9810843-5-1, pp. 177-184, 2008.

http://www.fz-juelich.de/nic-series/volume39

Density Functional Modeling of Magnesia Supported Pd Clusters: On the Road to an Understanding of Nanoscale Catalysis

B. Huber[1,2], P. Koskinen[1,3,4], H. Häkkinen[4], and M. Moseler[1,2,3]

[1] Faculty of Physics, University of Freiburg, Herrmann-Herder-Str. 3, 79104 Freiburg

[2] Freiburg Materials Research Center, Stefan-Meier-Str. 21, 79104 Freiburg

[3] Fraunhofer Institute for Mechanics of Materials IWM, Wöhlerstr. 11, 79108 Freiburg
E-mail: mos@iwm.fhg.de

[4] Department of Physics, NanoScience Center, University of Jyväskylä

Understanding and predicting heterogeneous catalysis remains one of the main motivations underlying the science of supported nano-cluster. Surface science experiments provide important insights into nano-particles catalysed reactions. Often however, this progress is only achieved in combination with quantum-chemical atomistic simulations. Here we show how density functional theory can be used to understand experimental size evolutionary patterns in the activity of metal-oxide supported Pd clusters. We provide theoretical evidence that the reaction of supported Pd_N with molecular oxygen results in the formation of nano-oxides which are in epitaxy with the ceramic support. These oxides serve as a Mars-van-Krevelen oxygen reservoir and therefore play an important role in the catalyzed combustion of carbon monoxide.

1 Introduction

Oxide-supported transition metal clusters and nanoparticles have recently attracted significant attention due to their important role as components of model-catalysts[1–6], sensors[7], solar-cells[8] and magnetic recording devices[9]. For small clusters, functionality and structure are closely interrelated. However, knowledge of the structure of the bare cluster is insufficient since the interaction with the chemical environment might cause drastic structural changes. Here we show by *ab initio* simulations based on the density functional theory that the reaction with molecular oxygen transforms small, non-crystalline, magnesia-supported Pd-clusters to crystalline Pd_xO_y nano-oxide clusters that are in epitaxy with the underlying support. Restructuring of the Pd backbone is controlled by the electrostatic interaction with magnesia leading to a strong reduction of the O_2 dissociation barrier. The supported Pd_xO_y clusters are likely to serve as Mars-van-Krevelen[10] oxygen reservoirs in catalytic oxidation reactions as observed previously for PdO overlayers[11] and demonstrated here for the oxidation of CO molecules.

The pronounced chemical activity of small metal clusters is due to a combination of several factors, with their relative contributions strongly depending on cluster size and elemental composition[3,12]. For transition metal clusters, the highest occupied valence orbital is generally close to or within a manifold of d-derived states, and the average position and the width of such d-band dictates much of the characteristics of adsorption of molecules via covalent bonding[13]. In gas-phase palladium clusters, the closed-shell $4d^{10}5s^0$ atomic configuration opens via significant s-d hybridisation, which induces a spin-magnetic moment[14]

and enhances the reactivity of small clusters. When adsorbed on alkaline supports, such as magnesia, surface defects serve as strong trapping centres for the clusters that maintain their open valence shells and finite spin-moments[15]. Model-catalytic experiments and *ab initio* simulations indicated that even a single Pd atom adsorbed at a surface colour centre (FC) of the magnesia support can be catalytically active for CO oxidation with a direct CO_2 formation from either molecularly adsorbed oxygen or from a Pd-carbonate-complex[16].

This contribution reports an extensive density functional theory (DFT) study of the oxidation of magnesia-supported Pd_N clusters (N=4-9)[17,18] revealing a novel, unexpected low-temperature oxidation mechanism, involving a phase of an epitaxially grown Pd_xO_y/MgO(FC) that functions as a catalytic centre for CO oxidation.

2 The Born-Oppenheimer-Spin-Density-Molecular-Dynamics-Method

We employ the work horse of large scale quantum chemistry namely Kohn's density functional theory[19,20]. This method plays a dominant role for large systems since it reduces the complicated many electron system to a more tractable picture of a single electron in the mean field of the other electrons resulting in a three-dimensional eigenvalue equation, the so called Kohn-Sham equation.

$$\left(-\frac{1}{2}\nabla^2 + v_{eff,\sigma}(\mathbf{r}) \right) \phi_{i,\sigma}(\mathbf{r}) = \epsilon_{i,\sigma}\phi_{i,\sigma}(\mathbf{r}). \tag{1}$$

Here the $\phi_{i,\sigma}$ are a set of a single particle electronic wave function, $\epsilon_{i,\sigma}$ their energies and the effective potential is given by

$$v_{eff,\sigma}(\mathbf{r}) = v(\mathbf{r}) + \int d^3r' \frac{n(\mathbf{r}')}{|\mathbf{r}-\mathbf{r}'|} + v_{xc,\sigma}(\mathbf{r}). \tag{2}$$

The electron density n of the system as the central quantity of density functional theory derives from the occupied Kohn-Sham orbitals $n(\mathbf{r}) = \sum_{i,\sigma}^{occ} |\phi_{i,\sigma}(\mathbf{r})|^2$. In order to make the computations less expensive only chemically active electrons are considered and therefore a pseudo potential v is used for the confinement of the valence electrons representing the influence of the naked ions and the core electrons[21]. The so called exchange-correlation potential v_{xc} takes into account many body effects that are not included in the classical Coulomb field $\int d^3r' \frac{n(\mathbf{r}')}{|\mathbf{r}-\mathbf{r}'|}$ in the above equation. It is treated in the framework of the local density approximation (LDA) and improved by the generalized gradient approximation[22]. The spin of the system is explicitely taken into account by calculating the wave functions of both spin manifolds $\sigma = \uparrow, \downarrow$ and thus the description of magnetism is possible within this formalism. For more details on spin density functional theory, the reader is referred to standard text books[20].

For large systems, this equation can be solved with great accuracy and efficiency using a plane wave basis for the single electron wave functions[23]. However, the required memory and CPU speed still exceeds modern serial hardware and thus massive parallel computing is the only way to solve the Kohn-Sham equations for a large number of atoms. For instance, for the description of a Pd_{13} cluster on an MgO(001) surface[15], we utilized 3D grids of the order of 200 grid points in each dimension for the Fourier and real space representation of approximatelly 200 electronic wave functions resulting in a memory consumption of the

order of 10 Gbyte! Thus the demanding computation of nanocatalysts could only be done after reception of a generous computer grant for the JUMP at the NIC Jülich.

The method for the numerical solution of eq. (1) utilizes the Born-Oppenheimer-local-spin-density-molecular-dynamics (BO-LSD-MD) approach of Barnett and Landman[23] and benefits from the fact that the differential operator $-\frac{1}{2}\nabla^2$ is a simple multiplication by $-\frac{1}{2}k^2$ for the Fourier transform $\phi_{\mathbf{k}}$ of the wave function. An iterative Block-Davidson eigenvalue solver only needs the action of the Hamiltonean $-\frac{1}{2}\nabla^2 + v_{eff}$ onto a wave function and therefore a dual space technique treating the kinetic energy in Fourier and the potential energy part in real space provides a very efficient scheme to solve eq. (1). A domain decomposition of both spaces and an efficient parallelisation of the fast fourier transform (FFT) conecting k- and real space results in a very good parallel efficiency on massively parallel machines like the NIC JUMP. The FFT is also used to calculate the Coulomb field $\int d^3r' \frac{n(\mathbf{r}')}{|\mathbf{r}-\mathbf{r}'|}$ since it satisfies Poissons equation which is algebraic and thus easily solvable in k-space. After the solution of the Kohn-Sham equations, the forces on the ions are calculated employing the Hellmann-Feynman-Theorem[20]. For more details on the numerical aspects of the method see[23].

The atomic and electronic structure of the active part of the supported Pd_N/MgO system (comprising the vicinity of the colour centre of the MgO(100) surface, the adsorbed Pd_N cluster, and the reactant molecules O_2 and CO) were calculated within the DFT in combination with the BO-LSD-MD (for details concerning pseudopotential and plane wave cutoff see ref.[17]). The MgO surface with the F-centre is modelled by a two-layer *ab initio* cluster $Mg_{13}O_{12}$, embedded in a point-charge lattice to model the long-rage Madelung potential. 2087 alternating charges of +2 and -2 of Mg and O ions, respectively, were used. In addition, those positive point charges that would be nearest neighbours to the periphery O atoms of the $Mg_{13}O_{12}$ cluster were replaced by empty Mg pseudopotentials (i.e. those Mg ions are represented by the same pseudopotential as the ones inside the active region, but they do not contribute electrons to valence) in order to prevent unphysical polarization of O ions. The lattice parameter of the embedding part is fixed to the experimental lattice constant (4.21 Å) of bulk MgO. For each cluster system Pd_N/MgO(FC) as well as for the further calculations with the reactant molecules, the Mg and O ions of the substrate are kept fixed to the ideal truncated bulk positions. The palladium part and the molecules are treated fully dynamical during steepest-descent-like optimisations starting from many initial configurations. The cluster's spin degree of freedom S was determined by a series of total energy $E(S_z)$ calculations with restricted spin z component (S_z). In general, $E(S_z)$ showed a plateau with a slight energy variation of 100 meV for $S_z = S$ followed by a sudden rise of several hundred meV for larger S_z (a similar behaviour was observed previously for gas-phase Pd clusters, see Ref.[14]). Consequently, we estimate that the accuracy of the total energies and hence the reported adsorption energies regarding the spin degree of freedom is within 0.1 eV. The minimum energy pathways and barriers of the O_2 dissociation reaction were calculated employing the nudged elastic band method[24] by using typically 5-9 images along the reaction path. The CO reaction pathways were obtained by constrained energy minimisation for a set of fixed distances between the carbon and the closest oxygen on the nano-oxide. Atomic charges and local magnetic moments were determined from the accumulated electron spin density within the domains of a Richards-Voronoi decomposition of space[25] using the ionic radii of the atoms.

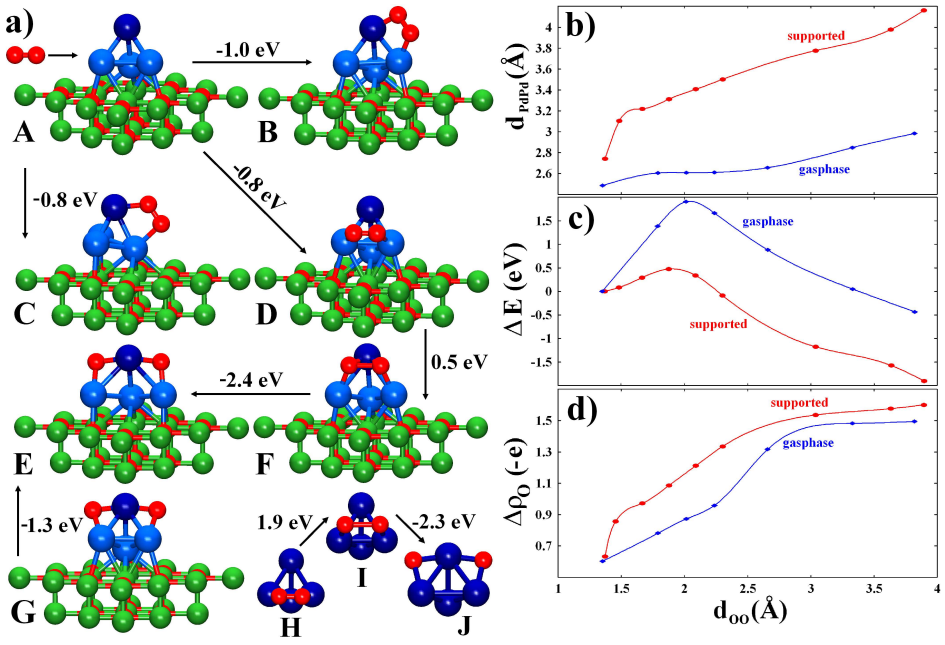

Figure 1. The oxidation of magnesia-supported Pd_4. Panel a) A: structure of the bare supported Pd_4; B-D: Pd_4 with moleculary adsorped O_2; E: ground state of Pd_4O_2/MgO(FC) with dissociated O_2; F: transition state between D and E. Oxygen atoms are represented by red, Mg by green, Pd atoms in contact with the substrate by light-blue and Pd in the second adlayer by dark-blue spheres. Arrows and numbers indicate transitions and energy differences between states. Panels b)-d): Nudged elastic band calculation of the pathways C→E and H→J. Shown are the Pd-Pd distance d_{PdPd}, the energy difference ΔE relative to the initial states and the charge accumulation $\Delta\rho_0$ on the oxygen as a function of the O-O distance d_{O-O}.

3 Results

The structures of the MgO-supported clusters were taken from an earlier DFT study[15] of Pd_N soft-landing on oxygen vacancies. The FCs represent the most prominent defects on MgO surfaces[27] and serve as pinning centres for the closest Pd atom (see Figs. 1a and 2). The other Pd atoms prefer neighbouring Mg-O bridges or form a second layer (light and dark blue atoms in Fig. 2, respectively).

The interaction of Pd_4/MgO(FC) with O_2 results in a barrierless metastable molecular adsorption on one of the three inequivalent Pd-Pd bridges with adsorption energies (E_{ad}) ranging between 0.8-1.0 eV (B-D in Fig. 1a). In the ground state (GS) of O_2Pd_4/MgO(FC), O_2 dissociates in the 2nd adlayer (E in Fig. 1a) with E_{ad} of 2.7 eV and a low dissociation barrier of 0.5 eV (Fig. 1a, F) with respect to a metastable molecular state (Fig. 1a, D). Note, that this activation barrier is considerably lower than the corresponding 1.0 eV barrier for room temperature O_2 dissociation on Pd(111)[28] implying that the reaction on Pd_N should be experimentally realised below room temperature. Interestingly, Pd atoms on the Mg-O bridges were displaced towards surface oxygen top positions creating a registry of Pd and O with the underlying support (E in Fig. 1a). This strong relaxation (as reflected in Pd-Pd distance in Fig. 1b) accompanies the dissociation indicating the importance of the

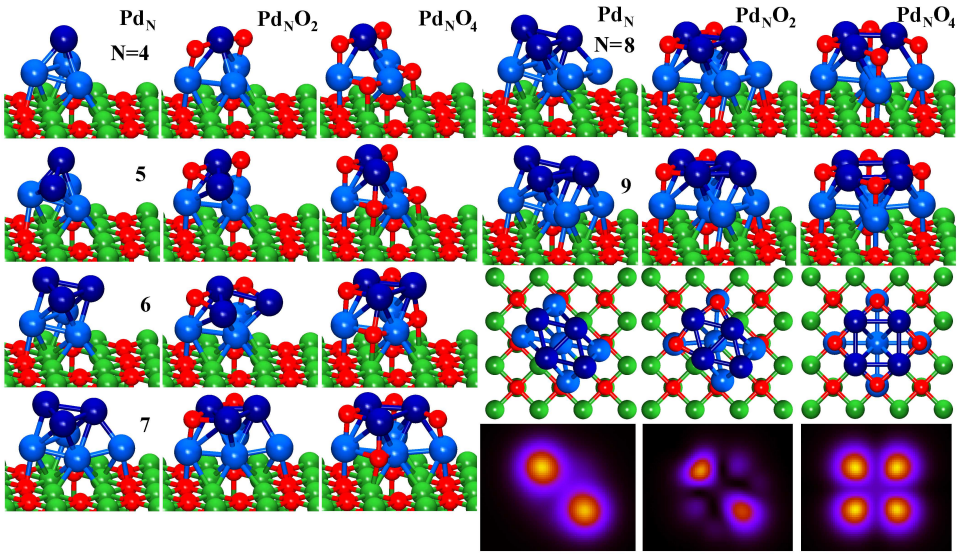

Figure 2. Structural growth motif of bare and oxidised Palladium clusters on MgO(FC). Panel in the right bottom corner: Tersoff-Hamann[26] STM simulation of supported O_xPd_9 assuming constant scan height of 2.5 Å above the cluster and contribution of orbitals within 0.2 eV below the Fermi energy.

structural fluxionality of the cluster. In fact, if Pd_4 were treated static during O_2 dissociation, the activation barrier would be 1.2 eV (see Fig.1a G for the final structure of the static Pd_4). Notably, no significant relaxation was observed for the oxidation of gas phase Pd_4[29] (Fig. 1a, reaction H→I→J). The cluster retained its tetrahedral shape during the reaction with a rather high activation energy of 1.9 eV (see Fig. 1b and 1c for a comparison of Pd-Pd distances and barriers pertaining to the gas phase and the supported reaction). This observation suggests that intra-cluster chemistry is unlikely to be the main driving force for the observed fluxionality.

The separation of the two oxygen atoms is accompanied by a significant electron transfer from Pd to O increasing the anionic charge from -0.6 e/O-atom for the molecular O_2 to -1.6 e/O-atom for the dissociated O_2 on the supported cluster and to -1.5 e/O-atom on the gas phase Pd_4 (Fig. 1d). Consequently, the supported oxidised Pd_4O_2 is influenced by a significant Madelung potential from the ionic substrate. We estimated the difference of the Madelung energies of the unrelaxed (Fig. 1a, G) and the relaxed Pd_4O_2 (Fig. 1a, E) employing a classical point charge model with charges and atomic positions taken from our DFT calculations. Within this model, the cluster gained 2.1 eV upon relaxation. This result compares rather well with the DFT energy difference of 1.3 eV (considering the neglect of bond breaking in the classical model).

Our calculations of the dissociation of M=1,2 O_2 molecules on the larger Pd_N clusters (N=5-9) revealed essentially the same processes as already discussed for Pd_4 resulting in a systematic growth pattern of $O_{2M}Pd_N$/MgO(FC) (Fig. 2). For all cluster sizes, the first pair of oxygen atoms was inserted in the 2nd adlayer epitaxially on O-sites of the magnesia with E_{ad} ranging between 2.7 eV and 3.4 eV. Notably, the optimum positions of the second

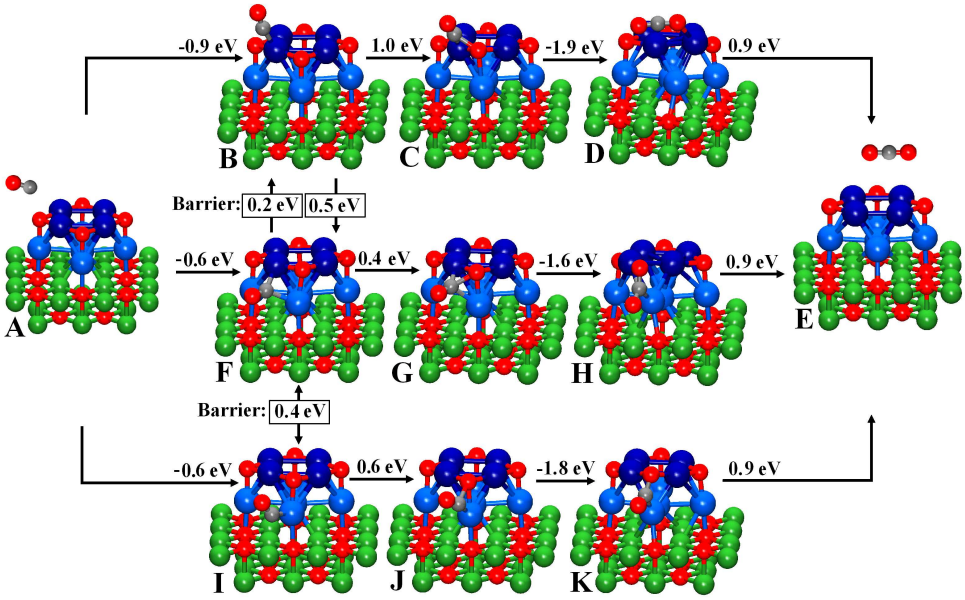

Figure 3. Possible CO oxidation reaction pathways A-B-C-D-E, A-F-G-H-E and A-I-J-K-E on O_4Pd_9/MgO(FC). Carbon is depicted as grey spheres. Structures (except transition states C, G and J) represent stable local minima. The transition state energies between B and F and between F and I are reported in boxes. After adsorption on B, the CO can take the direct route B-C-D (barrier 1.0 eV) or the indirect routes B-F-G-H or B-F-I-J-K having a multiple-barrier structure (0.5 eV/0.4 eV for the former and 0.5 eV/0.4 eV/0.6 eV for the latter) leading to effective barriers of 0.7-0.9 eV.

O pair showed a pronounced size-dependence. For smaller clusters (N=4-6) the 3rd and 4th oxygen atom occupy ideal MgO lattice sites in the first adlayer with reduced E_{ad} ranging between 1.6 eV and 1.8 eV. A structural transition occurs after Pd_6 leading to an O_4Pd_7/MgO(FC) with three oxygen atoms in the 2nd adlayer (E_{ad}=2.2 eV) and a complete depopulation of the 1st adlayer for Pd_8 and Pd_9 (E_{ad}=3.0 and 3.2 eV). The formation of a highly symmetric C_{4v} GS for O_4Pd_9/MgO(FC) produced a 2nd adlayer that is in perfect epitaxy with the MgO surface (see top view in Fig. 2). In principle, the transition from the C_{2v} Pd_9/MgO(FC) to the C_{4v} O_4Pd_9/MgO(FC) could be detected experimentally by scanning tunnelling microscopy (STM). In our simulated STM images (bottom row in Fig. 2) the rearrangement of the Pd atoms is clearly visible. Surprisingly, the square-like Pd_4O_4 unit in the completed 2nd adlayer represents the basic building block of a Pd(111) surface oxide[30]. Note however, that Pd(100) supports the formation of a $\sqrt{5} \times \sqrt{5}R27^\circ$ structure which has been interpreted as a (101) monolayer of tetragonal bulk PdO[31].

Recently, it has been demonstrated experimentally that PdO overlayers on Pd(100) can serve as Mars-van-Krevelen oxygen reservoirs for high temperature CO oxidation[11]. To elucidate the existence of a corresponding mechanism on Pd nano-oxides, we performed extensive DFT calculations of CO adsorption and CO_2 formation on O_4Pd_9/MgO(FC). The CO molecules adsorb preferentially on top of 2nd layer Pd atoms (structure B in Fig. 3 with E_{ads}=0.9 eV), on the Pd-Pd bridges (F in Fig. 3 with E_{ads}=0.6 eV) and at the side of the cluster close to the surface (I in Fig. 3 with E_{ads}=0.6 eV). The adsorption sites B,

F and I are interconnected by rather low barriers ($\leq$ 0.5 eV) indicating that CO molecules should be quite mobile on O_4Pd_9/MgO(FC) below room temperature.

We first describe CO_2 formation assuming low CO coverage i.e. the molecules get oxidized one at a time. At finite temperature, CO can be found at any of the three identified adsorption sites B, F or I. Site B can be reached either directly from gas-phase or through the metastable sites F and I that first trap CO via reverse spillover[32]. The reaction barrier for forming CO_2 via the direct route B-C-D is clearly the highest. The calculated barrier of 1.0 eV roughly corresponds to the lowest barriers for CO oxidation on bulk Pd(111)[33]. However, effective barriers of the order of only 0.7 to 0.9 eV exist for the indirect reactions B-F-G-H or B-F-I-J-K where both pathways have a multiple-barrier structure (Fig. 3). While the detailed comparison of reaction routes B-C-D, B-F-G-H and B-F-I-J-K would require quantitative information of the respective kinetic prefactors, it is reasonable to conclude that at low temperatures the indirect mechanisms B-F-G-H and B-F-I-J-K are likely to dominate. We note that the preformed CO_2 molecules are still relatively strongly bound to the catalyst (0.9 eV for each of the structures D, H or K), however, from the energetic point of view the reaction heat ($\geq$ 1.6 eV) should be sufficient to detach them to the gas phase[16].

At higher CO partial pressures, all the four equivalent CO adsorption sites B are populated. This full occupation of the first Pd-O layer makes the bridge adsorption site (F) unstable for CO, which in effect closes the reaction channel F-G-H and decouples channels B-C-D and I-J-K, but does not strongly modify the reaction barriers along these channels. Under this condition, the reaction can still quite effectively proceed along the low-barrier channel I-J-K for those CO molecules that reach the cluster via reverse spillover. Our calculations also show that repeated CO oxidation with the system $O_M Pd_9$/MgO(FC), M=3,2,1, is possible via reaction routes similar to the ones described above for M=4, suggesting a possible complete re-metallisation of the cluster. However, Pd_9/MgO(FC) strongly adsorbs CO molecules on top of Pd-Pd bridges with adsorption energies of 1.7 eV. This inhibits subsequent O_2 dissociation and poisons the catalyst. Hence, our results indicate that MgO-supported Pd clusters would catalyse CO oxidation best under O_2-rich conditions.

Our barriers for CO_2 formation (0.6-1.0 eV), are reasonable when compared to corresponding model catalyst experiments[3] with size-selected Pd_N/MgO(FC), where CO_2 was formed between 200-600 K.[34] Furthermore, the poisoning effect[34] observed for CO deposited prior to O_2 agrees well with our finding that pre-adsorption of CO inhibits subsequent O_2 dissociation.

Acknowledgments

We thank U. Heiz for the communication of unpublished results and fruitful discussions. This work was supported by the Deutsche Forschungsgemeinschaft, the Fraunhofer MAVO for Multiscale Materials Modelling (MMM) and the Academy of Finland (AF).

References

1. Chemisorption and Reactivity on Supported Clusters and Thin Films; Lambert, R. M., Pacchioni, G., Eds.; Kluwer: Dordrecht, 1997; p 395-424.

2. H. Grönbeck, Topics in Catalysis **28**, 59 (2004).
3. U. Heiz and W-D. Schneider, in *Metal Clusters at Surfaces*, edited by K.H. Meiwes-Broer (Springer, Berlin, 2000) p. 237-273 and references therein.
4. C. Becker and C.R. Henry, Surf. Sci. **352**, 457 (1996).
5. H.J. Freund, Adv. in Catal. **45**, 333 (2000).
6. S.H. Shaikhutdinov et al. *et al.*, Surf. Sci. **501**, 270 (2002).
7. J. Mizei et al., Thin Solid Films **391**, 209 (2001).
8. M. Westphalen et al., Sol. Ener. Mater. & Sol. Cells. **61**, 97 (2000).
9. S. Fukami, A. Ohno and A. Tanaka, Mater. Trans. **45**, 2012 (2004).
10. P. Mars and D.W. van Krevelen, Chem. Eng. Sci. **3**, 41 (1954).
11. B.L.M. Hendriksen et al., Surf. Sci. 552, 229-242 (2004).
12. Cluster of atoms and molecules, edited by H. Haberland (Springer, Berlin, 1994).
13. B. Hammer and J.K. Norskov, in Chemisorption and Reactivity on Supported Clusters and Thin Films; Lambert, R. M., Pacchioni, G., Eds.; Kluwer: Dordrecht, 1997; p 331-351.
14. M. Moseler at al., Phys. Rev. Lett, **86**, 2545 (2001).
15. M. Moseler, H. Häkkinen and U. Landman, Phys. Rev. Lett. **89**, 176103 (2002).
16. S. Abbet et al., Phys. Rev. Lett. **86**, 5950 (2001).
17. B. Huber et al., Nature Materials **5**, 44 (2006).
18. B. Huber and M. Moseler, EPJD online (2007).
19. W. Kohn and L.J. Sham, Phys. Rev. A **140**, 1133, (1965).
20. R. Parr and W. Yang, *Density functional theory of atoms and molecules* (Oxford university press, 1989).
21. N. Troullier, and J.L. Martins, Phys. Rev. B **43**, 1993 (1991).
22. J.P. Perdew et al., Phys. Rev. Lett. 77, 3865 (1996).
23. R. Barnett and U. Landman, Phys. Rev. B **48**, 2081 (1993).
24. G. Henkelman and H. Jonsson, J. Chem. Phys. **113**, 9978 (2000).
25. F.M. Richards, J. Mol. Biol. **82**, 1 (1974).
26. J. Tersoff and R. Hamann, Phys. Rev. Lett. **50**, 1998 (1983).
27. S. Abbet et al., J. Am. Chem. Soc. **123**, 6172 (2000).
28. A. Eichler, F. Mittendorfer and J. Hafner, Phys. Rev. B **62**, 4744 (2000).
29. B. Huber et al., Comp. Mat. Sci. **35**, 371 (2006).
30. E. Lundgren et al., Phys. Rev. Lett. **88**, 246103 (2002).
31. M. Todorova et al., Surface Science **541**, 101 (2003).
32. U. Heiz and E.L. Bullock, Mater. Chem. **14**, 564 (2004).
33. C.J. Zang and P. Hu, J. Am. Chem. Soc. **123**, 1166 (2001).
34. U. Heiz, A. Sanchez and S. Abbet, Chem. Phys. **262**, 189 (2000).